IEEE Access
Multidisciplinary | Rapid Review | Open Access Journal

Received July 21, 2019, accepted August 3, 2019, date of publication August 6, 2019, date of current version August 21, 2019.

Digital Object Identifier 10.1109/ACCESS.2019.2933525

A Robust State Estimator for Integrated Electrical and Heating Networks

HAIXIANG ZANG[1], (Member, IEEE), MINGHAO GENG[1], MINGFENG XUE[2], XIAOBO MAO[2], MANYUN HUANG[1], SHENG CHEN[1], (Student Member, IEEE), ZHINONG WEI[1], (Member, IEEE), AND GUOQIANG SUN[1]

[1]College of Energy and Electrical Engineering, Hohai University, Nanjing 210098, China
[2]Wuxi Power Supply Company of State Grid Jiangsu Electric Power Company Ltd., Wuxi 214002, China

Corresponding author: Haixiang Zang (zanghaixiang@hhu.edu.cn)

This work was supported in part by the National Natural Science Foundation of China under Grant 51877071, and in part by the Science and Technology Project of State Grid Jiangsu Electric Power Corporation under Grant J2019017.

ABSTRACT State estimation has been widely used in power system energy management systems. However, the application of state estimation for integrated electrical and heating networks (IEHNs) remains in a preliminary stage. This paper addresses this issue by proposing a robust state estimation method for IEHNs based on the weighted least absolute value in conjunction with equality constraints. The robust performance of the proposed estimator resolves the disadvantages of existing combined state estimators. A heating load pseudo-measurement model based on an artificial neural network and real-time measurements is developed to suppress the negative effects of measurements that contain bad data, and thereby ensure an adequate basis for accurate state estimation and guarantee the observability of the heating network. The effectiveness of the proposed state estimation method and its robustness to bad data are verified by comparison with the performance of the conventional largest normalized residual test based on the equality-constrained weighted least squares state estimation of IEHNs in numerical simulations employing a simple IEHN and/or the Barry Island IEHN as case studies.

INDEX TERMS Integrated electrical and heating network, state estimation, weighted least squares absolute value, pseudo-measurement model, bad data identification.

NUMENCLATURE

A. INDICES AND PARAMETERS

- $[\lambda]$ overall heat transfer coefficient per unit length W/(m·K)
- $[\eta]$ circulation pump efficiency
- $[g]$ gravitational acceleration (kg·m/s^2)
- $[c_m]$ heat-to-power ratio
- $[C_p]$ specific heat of water (J/(kg·K))
- $[L]$ pipe length (m)
- $[\boldsymbol{Y}]$ node admittance matrix
- $[Z]$ ratio describing the trade-off between heat supplied to a site and electrical power

B. VARIABLES

- $[m]$ mass flow rates within each pipe (kg/s)
- $[m_q]$ mass flow through each node injected from a source or discharged to a load (kg/s)
- $[m_{out}]$ mass flow rate within a pipe leaving a node (kg/s)
- $[m_{in}]$ mass flow rate within a pipe entering a node (kg/s)
- $[T_s]$ supply temperature (°C)
- $[T_r]$ return temperature (°C)
- $[T_o]$ outlet temperature prior to mixing in the the return network (°C)
- $[T_a]$ ambient temperature (°C)
- $[T_{out}]$ mixture temperature of a node (°C)
- $[T_{in}]$ temperature of flow at the end of an incoming pipe (°C)
- $[T_n]$ temperature at each node in a supply and return network (°C)
- $[T_{bt}]$ temperature prior to mixture at the end of each pipe (°C)
- $[h]$ pressure head (m)
- $[h_f]$ head losses within a pipe (m)
- $[h_c^{pu}]$ pump head of the heating network (m)

The associate editor coordinating the review of this manuscript and approving it for publication was Salvatore Favuzza.

$[H_n]$	pressure head at each node in a supply and return network (m)
$[V_i]$	the voltage at busbar i (p.u.)
$[\Phi_i]$	the heat power at node i (MW)
$[\Phi^{CHP}]$	useful heat output of CHP units (MW)
$[P^{CHP}]$	electrical power output (MW)
$[P^{Con}]$	electrical power generation of an extraction unit in full condensing mode (MW)
$[P^{pu}]$	electrical power consumed (MW)
$[\boldsymbol{z_e}]$	measurement vector in the electrical network
$[\boldsymbol{z_h}]$	measurement vector in the heating network
$[\boldsymbol{\varepsilon_e}]$	measurement vector error in the electrical network
$[\boldsymbol{\varepsilon_h}]$	measurement vector error in the heating network

C. CONSTANTS AND SETS

$[n_{pipe}]$	number of pipes in a heating network
$[n_{loop}]$	number of loops in a heating network
$[n_{Gd}]$	number of nodes in a heating network except the source node
$[\mathcal{I}^{node}]$	set of nodes in a heating network
$[\mathcal{I}^{pipe}]$	set of pipes in a heating network
$[\mathcal{I}^{loop}]$	set of loops in a heating network
$[\mathcal{I}^{Sd}]$	set of source nodes in a heating network
$[\mathcal{I}^{load}]$	set of load nodes and load nodes in a heating network
$[\mathcal{I}^{Gd}]$	set of nodes in a heating network except the source node
$[\mathcal{I}^{Id}]$	set of intermediate nodes in a heating network
$[\mathcal{N}^{zero}]$	set of zero-injection nodes in an electrical network

I. INTRODUCTION

Increasing energy constraints and environmental degradation have generated intense interest in improving the energy efficiency and increasing the penetration of renewable energy sources in energy networks. This has promoted the rapid development of integrated energy systems (IESs), which are also denoted as multi-energy systems [1]. Such systems generally combine at least two distinct energy networks, such as electrical and heating networks. For example, integrated electrical and heating networks (IEHNs) coupling combined heat and power (CHP) units, heat pumps, and boilers have been demonstrated to improve the economic performances of the two energy systems while meeting the general energy demands of end users with reduced environmental costs [2]. Furthermore, optimizing the supply of electrical power in terms of individual units also increases the flexibility of IEHNs for managing fluctuations in power supply arising from renewable energy sources.

Current research focused on IESs and IEHNs centers largely around system modeling, planning, scheduling, optimization, and evaluation [3]–[11]. Liu *et al.* [4] conducted foundational system modeling work by developing a model for IEHNs, and proposing a method for solving the combined heat and electrical power flow equations. Pan *et al.* [5] developed an economic dispatching scheme that considered the dynamic characteristics of IEHNs and the serviced buildings over time. Ren and Gao [9] developed a mixed-integer linear programming (MILP) model for the integrated planning and evaluation of distributed energy systems. However, online dispatch and control strategies depend on complete and reliable real-time data, which is generally rather limited in scope and unavoidably subject to bad data due to economic and technical reasons. This issue has been widely addressed in conventional electrical power systems by subjecting real-time measurements to a filtering process, and then applying state estimation (SE) to obtain the states of the entire system [12]–[16]. To this end, the weighted least absolute value (WLAV) state estimator has been often applied because of its excellent robust performance [17]–[19]. However, the application of SE for IEHNs remains in a preliminary stage. Among the available studies on this subject, an SE method focused on calculating heat loss was proposed in [20]. Dong *et al.* [21] proposed an SE approach for IEHNs, and applied the classic weighted least squares (WLS) method as the minimization function in the state estimator and the largest normal residual (LNR) for conducting bad data identification. However, the constraints of the heating network were not fully considered in the adopted steady-state IEHNs model. Sheng *et al.* [22] proposed an extended IEHN model that also considered the dynamics of pipelines, and applied a two-stage SE approach to solve the model. Zhang *et al.* [23] developed a decentralized algorithm based on the asynchronous alternating direction method of multipliers for integrated heat and power networks, in which the measurement information because the two networks is not shared. These studies demonstrated that, compared with applying SE to the individual systems independently, conducting SE for the combined systems of an IEHN provides higher SE accuracy by satisfying the constraints of the IEHN components coupling the two systems. In addition, it must be noted that SE requires that system measurements have an appropriate degree of redundancy. However, district heating networks generally lack real-time heat power measurement equipment. This has led to an intense interest in predicting the cold and heat power loads of IESs [24], [25]. For example, Shahaboddin *et al.* [25] constructed an adaptive neuro-fuzzy inference system to predict the heat loads of individual consumers in a district heating network. However, pure heat load forecasting methods must consider many factors, and the process is not closely related to existing real-time measurement data. Consequently, the accuracy of the SE based exclusively on heat load forecasting is limited, and more intelligent methods of estimating heat loads based on real-time measurements are required.

Although the advantages of conducting SE for the combined systems of an IEHN over that applied to the individual

systems independently have been demonstrated by the above-discussed studies, this approach suffers from the following significant disadvantages.

(1) Heating network constraints have not been fully considered in the IEHN model.
(2) The existence of bad data in the electrical network will affect the SE results of the heating network, and vice versa. Furthermore, the probability of obtaining bad data in heating network measurements is often greater than that in the electrical network because of the working environment and the automation level of thermal meters. Therefore, the combined SE of IEHNs requires robust performance.
(3) The lack of a full array of direct heat power measurements in the heating network makes many of the existing measurements in an IEHN critical, and the loss of any such critical measurement from the measurement set can make the IEHN unobservable.

The present work seeks to address these research gaps by making the following contributions.

(1) We apply robust WLAV-based SE to a steady-state model of an IEHN that considers the complete equality constraints, and compare the results with equality-constrained (EC) WLS in a simple IEHN and the Barry Island IEHN as numerical simulation test case studies.
(2) An artificial neural network (ANN) heating load pseudo-measurement model based on real-time measurements is developed to reduce the number of critical measurements in the heating network and guarantee the observability of the system. The accuracy of the model is verified by comparisons with the load profiles of an actual heating network.
(3) The robustness of the proposed method is verified by comparing its performance with that of the conventional LNR test based on the EC-WLS in numerical simulations of the Barry Island IEHN.

The remainder of this paper is organized as follows. The IEHN model is presented in Section II. The SE model is introduced in Section III. The proposed WLAV-based SE method and the results of the case studies are presented in detail in Sections IV and V, respectively. Section VI presents the conclusions and directions for future work.

II. INTEGRATED ENERGY SYSTEM MODEL

The application scenarios of IEHN are mainly the coupling of district electricity systems (DESs) and district heating systems (DHSs). Fig. 1 presents a schematic illustrating the structure of an IEHN. Models for the DES are relatively mature, and this paper adopts the three-phase model described elsewhere [14]. Existing heating network models include the static model, quasi-dynamic model, and full dynamic model [26]. The present work employs the static model for the heating network in accordance with the time scales of the networks considered.

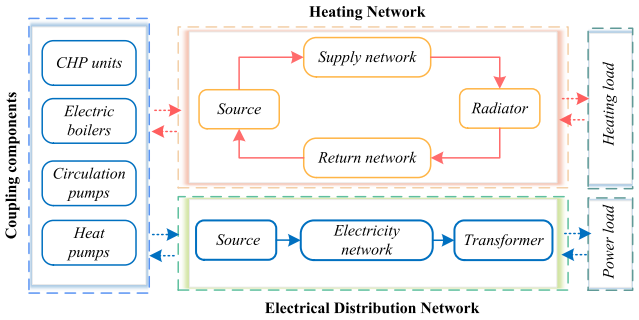

FIGURE 1. Schematic illustrating the structure of an IEHN.

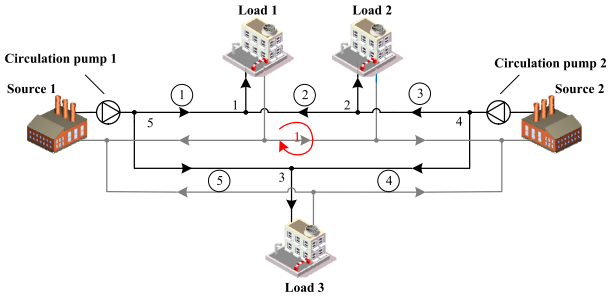

FIGURE 2. Structure of a simple heating network (case study 1).

Fig. 2 illustrates the structure of a simple heating network with two heat sources, two circulation pumps, and three load nodes denoted as 1, 2, and 3, and five pipelines denoted by the circled terms with supply pipelines given in black and return pipelines given in gray. The heating network is mostly tree-like, but it can include flow loops composed of, e.g., nodes 1, 2, 4, 3, and 5. A heating network is generally divided into a hydraulic model and a thermal model for analysis. In the hydraulic model, water or another thermal medium flows from the head to the end of a pipeline under a pressure difference created by circulation pumps at the heat sources that generate a head pressure. In the thermal model, heat is transferred from heat sources through the flow of the thermal medium to each load node. Therefore, the hydraulic and thermal models are coupled via the mass flow rates of the thermal medium. Changes in the heat load require adjustment of the heating system parameters. The parameters selected for adjustment depend on the regulation method adopted. These methods mainly include quality regulation, where the heat source outputs are adjusted, quantity regulation, where the total volume of the thermal medium in the system is adjusted, and intermittent regulation, where the number of heating hours is adjusted. At present, quality regulation is generally adopted for heating networks, and this is also applied in the present study. Therefore, the total volume of the thermal medium in the heating network and the number of heating hours are assumed to be constant. Thus, we assume that the mass flows in the supply pipelines and the return pipelines of the heating network are equal but opposite in direction for facilitating the analysis.

A. HYDRAULIC MODEL

The hydraulic model depicts the relationship between the mass flow rate and head pressure at different nodes. This relationship is governed by the following basic rules.

(1) The continuity of mass flow: the mass flow that enters into a node minus the mass flow that leaves the node is equal to the flow consumption at the node.

$$\sum m_{in} - \sum m_{out} = m_q \tag{1}$$

(2) Head loss equation: As the thermal medium flows along a pipe, the pressure drops due to friction. Thus, the relation between the flow and the head losses along each pipe is

$$h_f = Km\,|m| \tag{2}$$

where pipe resistance coefficient K is mainly determined by the mass flow rate and the pipe parameters [4].

(3) Loop pressure equation: the sum of head losses around a closed loop must equal to zero.

$$\sum h_f = 0 \tag{3}$$

B. THERMAL MODEL

The thermal model depicts the relationships among mass flow rates, temperature, and heat power. The heat power at the ith bus is calculated using the following equation.

$$\Phi_i = C_p m_{q,i}(T_{s,i} - T_{o,i}) \tag{4}$$

The relationship between the temperatures at both ends (i, j) of a pipeline (k) is calculated as follows.

$$T_j = (T_i - T_a)e^{-\frac{\lambda L_k}{C_p m_k}} + T_a \tag{5}$$

The temperature mixing equation is given as follows.

$$(\sum m_{out})T_{out} = \sum (m_{in}T_{in}) \tag{6}$$

As discussed, m provides the coupling between the hydraulic and thermal models. Meanwhile, m also has a direct relationship with the heat power of a CHP, which couples with the electrical network.

C. COUPLING COMPONENT MODEL

The coupling units considered include the CHP units and circulation pumps, which can be modeled as follows:

$$c_m = \Phi^{CHP}/P^{CHP} \tag{7}$$

$$Z = \frac{\Phi^{CHP} - 0}{P^{Con} - P^{CHP}} \tag{8}$$

$$P^{pu} = \frac{mgh_c^{pu}}{\eta}. \tag{9}$$

The electric boilers and heat pumps are modeled as coupling components elsewhere [4].

III. STATE ESTIMATION

The measurements in an IEHN are expressed as follows.

$$\begin{cases} z_e = \boldsymbol{h_e}(\boldsymbol{x_e}) + \boldsymbol{\varepsilon_e} \\ z_h = \boldsymbol{h_h}(\boldsymbol{x_h}) + \boldsymbol{\varepsilon_h} \end{cases} \tag{10}$$

Here, $\boldsymbol{x_e}$ and $\boldsymbol{h_e}(\boldsymbol{x_e})$, $\boldsymbol{x_h}$ and $\boldsymbol{h_h}(\boldsymbol{x_h})$ are the state variables and measurement functions in the electrical and heating networks, respectively. The mathematical model of the WLAV-based SE for an IEHN with equality constraints $\boldsymbol{c}(\boldsymbol{x_e}, \boldsymbol{x_h})$ is given as follows.

$$\begin{aligned} \min \quad & J(\boldsymbol{x_e}, \boldsymbol{x_h}) = \boldsymbol{w_e}^T\,|\boldsymbol{\varepsilon_e}| + \boldsymbol{w_h}^T\,|\boldsymbol{\varepsilon_h}| \\ s.t \quad & \boldsymbol{\varepsilon_e} = z_e - \boldsymbol{h_x}(\boldsymbol{x_e}) \\ & \boldsymbol{\varepsilon_h} = z_h - \boldsymbol{h_h}(\boldsymbol{x_h}) \\ & \boldsymbol{c}(\boldsymbol{x_e}, \boldsymbol{x_h}) = 0. \end{aligned} \tag{11}$$

Here, $\boldsymbol{w}_e$ and $\boldsymbol{w}_h$ are weighting vectors of the electrical and heating networks, respectively. In the following subsections, the SE of an IEHN is defined in detail by introducing state variables and measurement equations.

A. CHOICE OF IEHN STATES

The measurements in an electrical network can be expressed by voltage phasor in the form of polar coordinates. However, one of three possible combinations of state variables can be employed in a heating network [4], [20], and each has the distinct advantages and disadvantages listed in Table 1.

TABLE 1. Comparision of three state variable choices for heating networks.

State variables	Accuracy of calculation	Redundancy of measurements	Accuracy of calculation
(m, T_s, T_r)	Simple	High	High
(h, T_s, T_r)	Simple	High	low
(H_n, T_n, T_{bt})	Difficult	Low	High

According to the characteristics listed in Table 1, describing the state of the entire network via mass flow makes more intuitive sense. Furthermore, measurement redundancy is more important for conducting SE. Therefore, the state variables of the heating network in this paper are expressed by (m, T_s, T_r).

B. DESCRIPTION OF MEASUREMENTS

Communication in the electrical and heating networks is facilitated by a Supervisory Control and Data Acquisition (SCADA) system. The SCADA system collects all available real-time measurement data and uploads them to the energy management system. Along with the development of the distribution power systems, the measurement equipment is also increasing in its quantity, types, and precision. In addition to the branch power and branch current magnitude measurements that are common in distribution power systems, the node injected power and voltage magnitude can also be

obtained from smart meters. In the heating network, mass flow and temperature are the most common types of measurements, and nearly all pipes and nodes are configured for these measurements. Pressure measurements are also commonly obtained in a heating network, but the precision of pressure measurements is greatly affected by the environment. Finally, real-time heat power measurements are generally configured only at key nodes, such as heat sources or heat exchange stations. As such, common heat load nodes typically lack real-time heat power measurements, and only the total heat consumption of the network over a single day period is usually determined.

The measurement functions of the actual measurement system in a heating network for the hydraulic and thermal model are given as follows.

$$m_b = m_b \quad \forall b \in \mathcal{I}^{pipe} \tag{12}$$

$$m_{q,i} = \sum_{b \in \mathcal{I}^{pipe}} A_{ib} m_b \quad \forall i \in \mathcal{I}^{node} \tag{13}$$

$$h_{f,b} = K_b m_b |m_b| \quad \forall b \in \mathcal{I}^{pipe} \tag{14}$$

$$\Phi_i = C_p m_{q,i} (T_{s,i} - T_{o,i}) \quad \forall i \in \mathcal{I}^{Sd} \tag{15}$$

$$T_{s,i} = T_{s,i} \quad \forall i \in \mathcal{I}^{load} \tag{16}$$

$$T_{r,i} = T_{r,i} \quad \forall i \in \mathcal{I}^{load} \tag{17}$$

$$T_{r,i} = f(m, T_r) \quad \forall i \in \mathcal{I}^{Sd} \tag{18}$$

We also include the measurement function

$$\Phi_i = C_p m_{q,i} (T_{s,i} - T_{o,i}) \quad \forall i \in \mathcal{I}^{load} \tag{19}$$

if there are real-time heat power measurements or pseudo measurements in load nodes.

It is noted that to describe the measurement functions in brief, we use the node-branch incidence matrix $\boldsymbol{A}$ and loop-branch incidence matrix $\boldsymbol{B}$ in the measurement functions and the following constraint equations. The detailed explanations of $\boldsymbol{A}$ and $\boldsymbol{B}$ are shown in Appendix A.

Finally, a standard technique employed in electrical power systems is extended to the IEHN to avoid numerical problems such as ill-conditioned matrices [21].

C. PROBLEM STATEMENTS

The description of the above SE model and measurement functions illustrates that some differences between the heating and electrical networks lead to some problems. (1)

1) A comparison of measurement functions (12)–(18) with the thermal model equations (4)–(6) indicates that (5) cannot be obtained from the available measurements. Hence, the available measurement functions cannot fully characterize the heating network.
2) A comparison of measurement functions (12)–(15) with the hydraulic model equations (15)–(18) indicates that fewer equations exist for T_s and T_r than equations for m, and only temperature measurement equations (16)–(17) are available for solving T_s and T_r in most instances. These factors produce many critical measurements in the heating network, where the loss of a critical measurement can result in an unobservable system, which would greatly affect the accuracy of the state estimator.

These two factors produce many critical measurements in the heating network, where the loss of a critical measurement can result in an unobservable system, which would greatly affect the accuracy of the state estimator. To counter these problems, the pseudo-measurement model of heat power is constructed and the equality constraints are added into the SE model.

IV. PROPOSED METHODOLOGY

The proposed method consists of the pseudo-measurement model based on an ANN and the WLAV-based state estimator.

A. PSEUDO-MEASUREMENT MODEL

Numerous factors affect the heat load of a heating network, such as real-time price, daytime characteristics (weekday/weekend), historical data, and the production periods of factories using thermal energy. As a result, heat power predictions cannot be expressed as an explicit formulation that considers all of the related factors. Therefore, an ANN is employed for pseudo-measurement modeling of the heat power at load nodes. The essence of the method is to approximate a nonlinear high-dimensional function through back propagation (BP) networks [27].

The pseudo-measurement model adopts a three-layer feedforward ANN that includes an input layer, hidden layer, and output layer. The hidden layer uses sigmoid transfer functions, and the output layer uses linear transfer functions. Theoretically, the feedforward ANN can achieve arbitrary nonlinear mapping with a single hidden layer by appropriately selecting the number of neural nodes.

The inputs of the ANN are the real-time correlation measurements of the load nodes and the historical heating network state variables of all the nodes in the heating network, and the outputs are the real-time heat power of the pseudo-measurement nodes. The data of the actual heating network are divided into a training set and several testing sets. In addition, noise set samples accounting for 10% of the total training set are added into the training set to improve the output accuracy of the network when bad data occur in the input. Here, the presence of bad data in the actual measurement system is simulated by adding 5% bad data randomly in the real-time correlation measurement of each sample of the noise set.

The efficiency of network training is improved by reducing the dimension of the ANN input via the use of mutual information, which is derived from the concept of entropy in information theory to represent the extent to which information is shared among multiple variables. As such, mutual information is often used as a tool for variable selection [26]. This process enables the pseudo-measurement model to be applied to the real-time state estimator. The mutual information between discrete random variables X and Y

is defined as

$$I_{(X,Y)} = \sum_{i=1}^{N}\sum_{j=1}^{M} p(x_i, y_i) log_2(\frac{p(x_i,y_i)}{p(x_i)p(y_i)}), \quad (20)$$

where N and M are the number of samples of random variables X and Y, respectively. Large mutual information values indicate strong correlations between variables.

The number of nodes in the hidden layer is determined by comparing the training time employed for the ANN and the accuracy of the ANN predictions based on experiments. Overfitting of the ANN is avoided by conducting prediction error tests for different randomly selected test sets. This ensures that no large prediction error is obtained when new measurement data are used as the input.

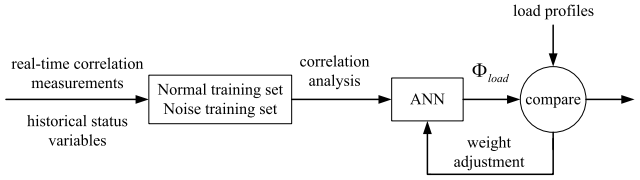

FIGURE 3. Schematic illustrating the process of ANN training.

The training process of the proposed ANN is illustrated in Fig. 3. In this work, the ANN is trained via the scaled conjugate gradient BP optimization method, which is suitable for large-scale problems. The ANN training process includes the following steps:

Step 1: generate the training and testing sets by combining the state information and real-time measurements, and add the noise set samples to the training samples;

Step 2: reduce the dimension of the ANN input by applying mutual information;

Step 3: use the heating load data as the target output of the ANN;

Step 4: train the network and adjust parameters including the number of neural nodes in the hidden layer according to the obtained prediction error and training time;

Step 5: save the difference between the ANN target output and the ANN actual output for further processing.

B. STATE ESTIMATOR

1) SOLUTION METHODOLOGY OF THE STATE ESTIMATOR

The proposed state estimator is solved using the primal-dual interior point method (PDIPM) [17]. The PDIPM has obvious advantages in dealing with large-scale optimization problems. A flowchart of SE execution is presented in Fig. 4. In addition, the following points must be noted in the combined SE of the IEHN.

(1) The state variables of the electrical and heating networks influence each other in the calculation. As a result, convergence is more rapid, and the impact of bad data is broader.

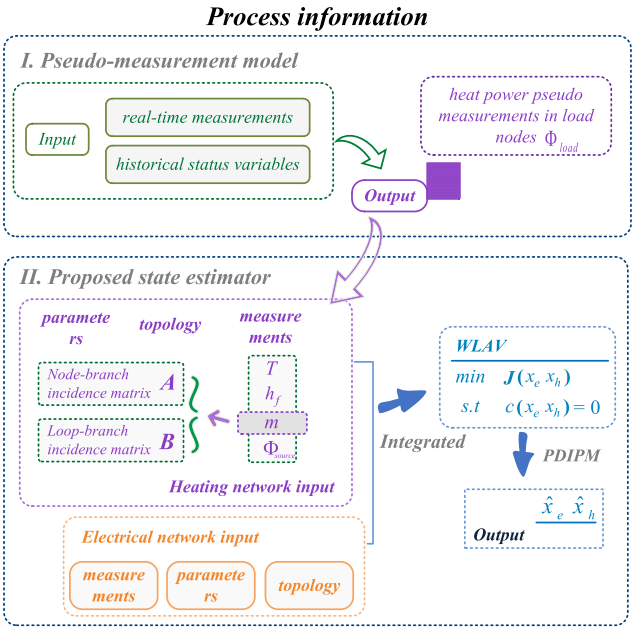

FIGURE 4. Flowchart of the proposed state estimation execution.

(2) The mass flow directions of the thermal medium in the pipelines are determined according to the measured mass flow data. This yields the node-branch incidence matrix $\boldsymbol{A}$ and the topology of the heating network. The incidence of bad data in the mass flow measurements will require the modification of $\boldsymbol{A}$ and affect the subsequent calculations of the constraint equations in the SE.

2) CONSTRAINT EQUATIONS

The constraints in the IEHN can be divided into five components.

(1) For the zero-injection bus in electrical network, the following constraints should be satisfied:

$$c_1(x) \equiv real\left\{(V_i \sum_{k\in\mathcal{N}^{bus}} (Y_{ik}V_k)^*)\right\} = 0 \quad \forall i \in \mathcal{N}^{zero} \quad (21)$$

$$c_2(x) \equiv imag\left\{(V_i \sum_{k\in\mathcal{N}^{bus}} (Y_{ik}V_k)^*)\right\} = 0 \quad \forall i \in \mathcal{N}^{zero}. \quad (22)$$

(2) Based on (5) and (6), we can establish a temperature constraint between the adjacent nodes in the heating network. The supply / return temperature mismatches are obtained:

$$c_3(x) \equiv \sum_{k\in\mathcal{I}^{Gd}} A_{s,ik}T'_{s,i} - b_{s,i} = 0 \quad \forall i \in \mathcal{I}^{Gd} \quad (23)$$

$$c_4(x) \equiv \sum_{k\in\mathcal{I}^{Gd}} A_{r,ik}T'_{r,i} - b_{r,i} = 0 \quad \forall i \in \mathcal{I}^{Gd}. \quad (24)$$

Here, we applied coefficient matrices $\boldsymbol{A}_s$ and $\boldsymbol{A}_r$, the vectors $\boldsymbol{b}_s$ and $\boldsymbol{b}_r$ for brevity. The expression of the temperature constraints (23–24) are detailed in Appendix B.

(3) From (2) and (3), we can reach loop pressure constraints if there are loops in the heating network:

$$c_5(x) \equiv \sum_{b\in\mathcal{I}^{pipe}} B_{ib}K_b m_b |m_b| = 0 \quad \forall i \in \mathcal{I}^{loop}. \tag{25}$$

(4) There are also zero-injections m_q or Φ constraints in heating networks:

$$c_6(x) \equiv \sum_{b\in\mathcal{I}^{pipe}} A_{ib}m_b = 0 \quad \forall i \in \mathcal{I}^{Id}. \tag{26}$$

(5) At the Electrical-Thermal coupling nodes, the coupling component constraints are given by:

$$c_7(x) \equiv P_i - \zeta\Phi_i = 0 \quad \forall i \in \mathcal{I}^{Sd} \tag{27}$$

where ζ is the value of coupling coefficient, determined according to the parameter of the specific coupling components (CHP units, electric boilers, heat pumps, or circulation pumps).

V. SIMULATION STUDY

The accuracy and robustness of the proposed method were tested for the simple IEHN shown in Fig. 2 (case 1) and the Barry Island case (case 2) shown schematically in Fig. 5 which is composed of an IEEE 34-bus electrical network and 32-node heating network. The detailed parameters of the two cases are presented elsewhere [4].

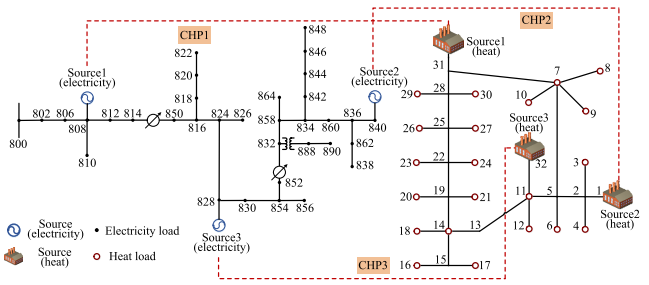

FIGURE 5. Schematic illustrating the barry island IEHN (case study 2).

A. EFFECTIVENESS OF THE PSEUDO-MEASUREMENT MODEL

The accuracy of the pseudo-measurement model was verified by its application to real-world data derived from an actual heating network over a six-month period. The heating load data for 21 nodes of the actual heating network is brought into case study 2. Here, it is assumed that all load nodes are configured with pseudo-measurements, and the heating network data were obtained by the anaysis of heating networks calculation in MATLAB [4].

The real-time correlation measurements are obtained by adding random errors to the calculated results, and the historical state variables are obtained by the state estimator. The target outputs are the heating load data for the 21 nodes. They were saved as the basis for ANN training and comparison. We selected 1200 sets of training samples (200 sets per month) from the heat load data, and 600 sets of testing samples (100 sets per month) were used for validation.

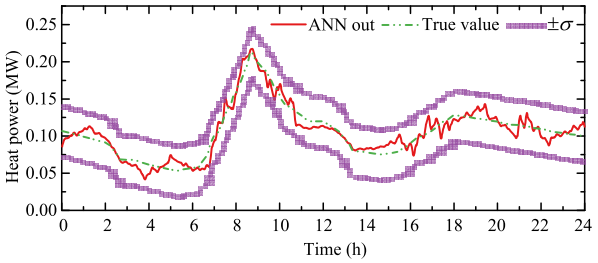

FIGURE 6. Day load curve prediction of heat power Φ_3.

TABLE 2. Statistical prediction accuracy of the ANN for the barry island case.

Month	11	12	1	2	3	4
AEP (%)	4.74	4.63	4.29	4.01	4.27	4.45

The day-load prediction value of the pseudo-measurement model for Φ_3 along with its true value and its $\pm\sigma$ confidence bounds are shown in Fig. 6. It can be seen that the proposed method can track the overall trend of the heat power and the overall error can be controlled within one standard deviation. The performance of the pseudo-measurement model was also quantitatively evaluated based on the average relative error percentage (AEP) defined as follows:

$$AEP = \frac{1}{n}\sum_{i=1}^{n}\left|\frac{\Phi_{p,i} - \Phi_{true,i}}{\Phi_{true,i}}\right| \times 100\%, \tag{28}$$

where n is the number of test samples, $\Phi_{p,i}$ is the output of the ANN, and $\Phi_{true,i}$ is the true value of the nodal heat power from the load profiles. The AEP values of the ANN output for six one-month periods are listed in Table 2. It can be seen from the table that the AEP values of the pseudo-measurements are uniformly less than 5%. Therefore, we conclude that the accuracy is sufficient for application to the state estimator.

B. PERFORMANCE OF STATE ESTIMATOR

We first analyze the performances of the EC-WLS-based SE method and the proposed WLAV-based state estimator from the perspectives of both the filtering effect and state variable estimation precision. The results of power flow calculations of the IEHN are taken as the true values x_{true}. The filtering effect is evaluated as the ratio of the normalized average estimation error S_H to the normalized average measurement error S_M, which are given as follows:

$$S_M = \frac{1}{M}\sum_{j=1}^{M}\left[\frac{1}{N}\sum_{i=1}^{N}\left(\frac{z_{i,t} - h_i(x_{true})}{\sigma_i}\right)^2\right]^{\frac{1}{2}}$$
$$S_H = \frac{1}{M}\sum_{j=1}^{M}\left[\frac{1}{N}\sum_{i=1}^{N}\left(\frac{h_{i,t}(x_{se}) - h_i(x_{true})}{\sigma_i}\right)^2\right]^{\frac{1}{2}}. \tag{29}$$

Here, M is the number of tests, N is the number of measurements, $z_{i,t}$ is generated by adding Gaussian noise with

TABLE 3. Comparison of statistical results for the two SE methods under scenario 1A.

	Alogorithm	Electrical network				Heating network				Time (s)
		S_M	S_H	S_H/S_M	$e_x(\%)$	S_M	S_H	S_H/S_M	$e_x(\%)$	
Case 1	WLS	0.9924	0.5712	57.56%	0.2551	0.9905	0.5133	51.82%	0.1433	0.0041
	WLAV	0.9924	0.6017	60.63%	0.2721	0.9905	0.5377	54.29%	0.1833	0.0110
Case 2	WLS	0.9943	0.4742	47.69%	0.2027	0.9927	0.3542	35.68%	0.0941	0.0089
	WLAV	0.9943	0.5455	54.86%	0.2612	0.9927	0.3722	37.49%	0.1068	0.2044

TABLE 4. Comparison of statistical results of two scenarios under the actual measurement configurations.

Scenario	Electrical network				Heating network				Number of critical measurements	Time (s)
	S_M	S_H	S_H/S_M	$e_x(\%)$	S_M	S_H	S_H/S_M	$e_x(\%)$		
2A	0.9941	0.5501	55.33%	0.2687	0.9921	0.4072	41.04%	0.1073	54	0.2103
3A	0.9941	0.5486	55.19%	0.2643	0.9923	0.3801	38.30%	0.1033	33	0.2175

standard deviations σ_i in the range of 0.01–0.05 to the true value in each test, and $h_{i,t}(x_{se})$ is the estimated value in each test. Under normal measurement conditions, S_M approaches 1 with an increasing number of experiments. The magnitude of the filtering effect decreases with decreasing S_H/S_M. The state variable estimation precision is evaluated by the average relative error:

$$e_x(\%) = \frac{100}{M}\sum_{j=1}^{T}\left(\frac{1}{N}\sum_{i=1}^{N}\left|\frac{x_{i,t}-x_{true}}{x_{true}}\right|\right)\times 100\%. \tag{30}$$

These values obtained by the SE methods based on the WLS and WLAV are compared for the two test cases under idealized measurement system configuration conditions, denoted as scenario 1A. In addition, we compare these values obtained by the proposed WLAV-based SE method for case 2 under realistic measurement configuration conditions, where the state estimator lacks heat load measurements at all of the load nodes. Here, we consider two scenarios, which include scenario 2A, where pseudo-measurements are not available, and scenario 3A, where the state estimator is configured with pseudo-measurements at all load nodes. The detailed measurement information are provided in Appendix C. All results were obtained after performing 2000 experiments.

The results of the SE methods based on the WLS and WLAV for the two cases under full measurement system configurations are listed in Table 3. The results indicate that the accuracy of WLAV-based SE is close to that of WLS-based SE in the absence of bad data. The results of the proposed WLAV-based SE method for case 2 under realistic measurement system configurations for the two scenarios are listed in Table 4. It can be observed that the performance of the WLAV state estimator is enhanced by the pseudo-measurements. The number of critical measurements is also reduced significantly.

C. ROBUSTNESS AGAINST BAD DATA

The robustness of the WLAV-based SE to bad data in IEHN measurements was tested for case 2 by adding bad data in accordance with various bad data ratios accounting for 0–10% of the total measurement data. The measurement configuration is the same as Scenario 3A. Here, bad data that were set to 130% of the true measurement value were randomly divided between the electrical network and the heating network, and 2000 example groups were randomly constructed for each bad data ratio. The robustness of the algorithm was evaluated using the mean estimation error S_{mean} and the maximum estimation error S_{max} defined as follows:

$$\begin{aligned} S_{mean} &= \frac{1}{M}\sum_{j=1}^{M}\left[\frac{1}{I}\sum_{i=1}^{I}\left|x_{se}^{i}-x_{true}^{i}\right|\right] \\ S_{\max} &= \frac{1}{M}\left[\max_{i=1}^{I}\left|x_{se}^{i}-x_{true}^{i}\right|\right]. \end{aligned} \tag{31}$$

Here, I is the number of state variables in. The simulation results of S_{mean} and S_{max} obtained for the five state variables (i.e., voltage magnitudes and angles of the electrical network, and source and return temperatures, and mass flow rates of the heating network) with respect to the bad data ratio are shown in Figs. 7–9. Generally, S_{mean} is used to evaluate the influence of bad data on the overall SE results, and S_{max} measures the local influence of bad data on SE results.

The results indicate that the proposed method can control the mean estimation errors within an order of magnitude of 10^{-3} with an increasing bad data ratio. However, the mean estimation errors of the mass flow are relatively large because the accuracy of measurements in the hydraulic model is low. In addition, the mass flow SE accuracy is more sensitive to bad data because of its strong correlations in the hydraulic model. Nonetheless, the proposed method

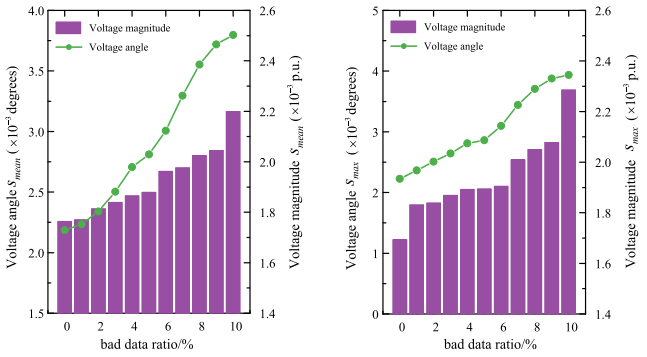

FIGURE 7. Values of S_{mean} and S_{max} of voltage with respect to the bad data ratio.

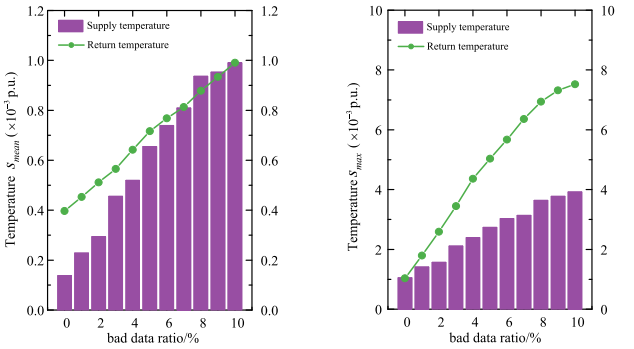

FIGURE 8. Values of S_{mean} and S_{max} for supply and return temperatures with respect to the bad data ratio.

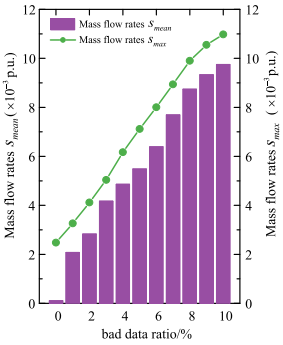

FIGURE 9. Values of S_{mean} and S_{max} for mass flow rates with respect to the bad data ratio.

demonstrates strong robustness to bad data and is therefore very suitable as a state estimator for the combined IEHN.

Bad data identification is one of the main functions of a state estimator. A robust state estimator can automatically identify bad data by comparing the estimation results with the measurements. Therefore, we conduct bad data identification after running the SE program, and any identified bad data is removed or corrected before conducting the next SE.

We compared the bad data identification performance of the proposed method (denoted as method 3) for case 2 with those obtained with two other methods. Here, method 1 adopts an WLS estimator, but does not take IEHN constraints into account [21]. Method 2 is based on the Lagrange estimator in conjunction with WLS that considers IEHN equality constraints (i.e., the EC-WLS estimator). Both methods 1 and 2 use the LNR sequence r_i^N to identify bad data. The Lagrange estimator based on WLS can be rearranged to obtain the correction equation of the Lagrange estimator as follows:

$$\left[H^T WH + \rho \nabla c(x)^T \nabla c(x)\right] dx = H^T W \Delta z^{(k)} - \pi \nabla c(x)^T c(x^{(k)}), \tag{32}$$

where $\boldsymbol{H}$ is the Jacobian matrix of the measurement functions, $\boldsymbol{W}$ is the weighting matrix, and π is the weighting factor of the constraint equations, which is much greater than any W_{ii}. A detailed derivation is presented elsewhere [12], [29]. This processing allows the LNR method to be applied to the EC-WLS estimator, and no numerical problems arise in the iterative process compared with an alternative method that treats the constraint equations as virtual measurements.

The LNR identification threshold was set to 3 according to a confidence of 99% [12]. The performances of the three bad data identification methods were compared using the following five scenarios.

(1) Three scenarios with a single bad data point
Scenario 1B: 130% of the true active power injection measurement at node 3 (P^A_{814}) is taken as bad data in the electrical network.
Scenario 2B: 130% of the true pressure measurement at node 3 ($h_{f,3}$) is taken as bad data in the heating network.
Scenario 3B: 130% of the true supply temperature measurement at node 6 ($T_{s,6}$) is taken as bad data in the heating network (this is a critical measurement).

(2) Two scenarios with multiple bad data points
Scenario 4B: bad data with weak correlation in the IEHN (Q^A_{814}, $P^B_{816-824}$, P^A_{844}, Φ_7, Φ_{20}, $h_{f,1}$) are set to zero. Scenario 5B: bad data with strong correlation in the IEHN (m_7 and $h_{f,7}$) are set to zero.

Table 5 presents the bad data identification results for the three methods. Method 1 failed in Scenario 3B because the residuals of critical measurements are always zero. Method 2 avoided this problem by applying the constraint equations. In addition, both methods 1 and 2 failed to identify the strongly correlated bad data in Scenario 5B, which occures often in the case of heating networks owing to the commonly high correlation between the measurements. The bad data resulted in the contamination of the residuals in the measurements, as shown in Fig. 10. In conclusion, when interacting or correlated bad data exists, the state estimator must also rely on the robust performance of the WLAV.

D. COMPUTATIONAL EFFICIENCY

The computational performance of the proposed state estimator was tested for case study 2 in the following three scenarios.

(1) Scenario 1C: WLS state estimator without bad data in the actual measurement system as a comparison benchmark.

TABLE 5. Bad data identification results for the five scenarios.

Scenario	Number of bad data points		Bad data rejected (yes/no))		
	Electrical network	Heating network	Method 1	Method 2	Method 3
1B	1	–	yes	yes	yes
2B	–	1	yes	yes	yes
3B	–	1	no	yes	yes
4B	3	3	yes	yes	yes
5B	0	2	no	no	yes

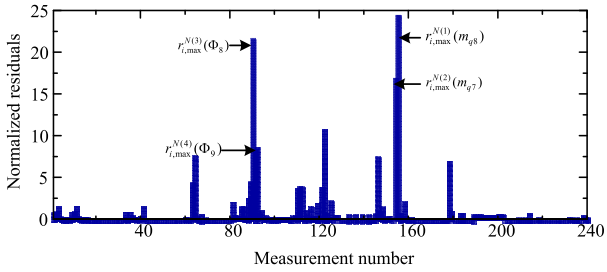

FIGURE 10. Normalized distribution of residuals in scenario 5B.

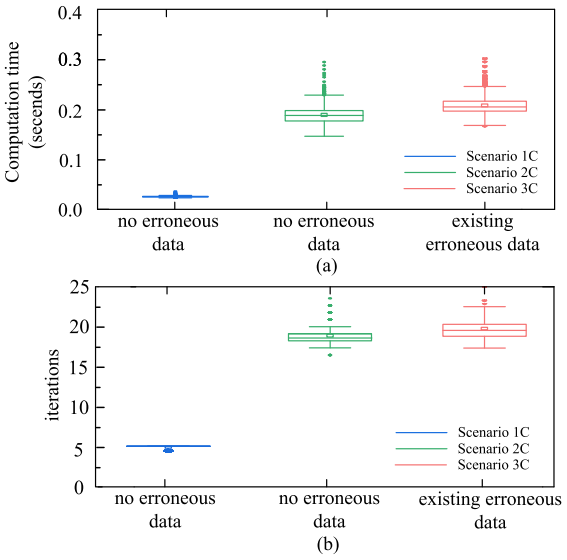

FIGURE 11. Computational performances under three scenarios.

(2) Scenario 2C: proposed state estimator without bad data in the actual measurement system.
(3) Scenario 3C: proposed state estimator with 5% bad data in the actual measurement system.

The results for the three scenarios are presented in Fig. 11. These results indicate that the computation speed of the proposed estimator is less than that of the WLS-based estimator, but it still meets the requirements of a real-time state estimator. In addition, the computational performance of the proposed estimator is nearly unaffected by bad data. Therefore, the proposed estimator sacrifices some degree of computational efficiency to ensure excellent robustness.

VI. CONCLUSION

As basic research in support of IES-SE, this paper proposed a robust SE method for an IEHN based on a pseudo-measurement model. The proposed method ensures the observability of the IEHN when the measurement system of the IEHN includes bad data, and thereby reduces the number of critical measurements for the heating network and improves the SE accuracy while satisfying all of the IEHN constraints compared with SE in the absence of the pseudo-measurement model. Moreover, good robust performance was demonstrated when bad data exist in the measurement system of the IEHN. It must be noted that these characteristics of the proposed method are essential for ensuring accurate performance of the energy management system of an IEHN. Future IEHN-SE-related research will seek to capitalize on the great practical value of considering the decoupling of mass flow and temperature estimations in the heating network. Furthermore, the dynamic SE of IEHNs under conditions of heating network state mutation is also a worthy research subject.

APPENDIX A
INCIDENCE MATRIX

(*i*) The node-branch incidence matrix $\boldsymbol{A}$ is defined with n_{node} rows and n_{pipe} columns. Each element of $\boldsymbol{A}$ describes

$+1$, if the flow in a pipe come into a node;
-1,if the flow in a pipe leaves a node;
0, if no connection from a pipe to a node.

(*ii*) The loop-branch incidence matrix $\boldsymbol{B}$ is defined with n_{loop} rows and n_{pipe} columns. Each element of $\boldsymbol{B}$ describes

$+1$, if the flow in a pipe is the same direction as the definition;
-1, if the flow in a pipe is the opposite direction as the definition;
0, if a pipe is not part of the loop.

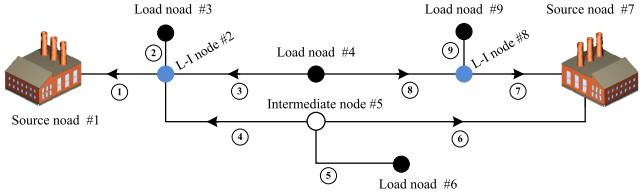

FIGURE 12. Different types of nodes in a return water pipe network.

APPENDIX B
TEMPERATURE CONSTRAINT EQUATIONS

We illustrate the temperature constraints (23) and (24) with an example based on the return pipeline network shown in the Fig. 12, where the nodes are numbered and the pipeline

numbers are placed within circles.The nodes in the heating network can be divided into the following four types.

(1) Source node: nodes with corresponding heat sources (nodes 1 and 7), which often represent the starting points of a heating network.
(2) Load node: nodes with heat loads (nodes 3, 4, 6 and 8), which often represent the terminal points of a heating network.
(3) Intermediate node: nodes without heat loads in the middle of the pipelines in a heating network (node 5).
(4) Load-intermediate node: nodes connected with a heat load in the middle of a pipeline of a heating network (node 2 and 9).

By analyzing all the nodes except the source nodes, n_{Gd} temperature constraint equations can be listed respectively. It is noted that there are differences of constraint equations among the three node types.

(*i*) Based on (5) and (6), we can express (24) when applied to load node 4 and intermediate node 5 respectively as follows.

$$T'_{r4} = T'_{o4} \tag{33}$$

$$-(m_4 + m_6)T'_{r5} + m_5 T'_{r6}\psi_5 = 0. \tag{34}$$

For brevity, we have applied the terms $T' = T - T_a$ and $\psi = e^{-\frac{\lambda L}{C_p m}}$. The terms with and without T_r are placed at the two sides of the equation, respectively.

(*ii*) Distinguishingly, the expression of (24) when applied load and intermediate node 2 is given as:

$$m_1 T'_{r2} - m_2 T'_{r3}\psi_2 - m_3 T'_{r4}\psi_3 - m_4 T'_{r5}\psi_4 = (m_1 - m_2 - m_3 - m_4)T'_{o2}. \tag{35}$$

All of the other temperature constraint equations can be extrapolated from (33)–(35). We can get (23) and (24) by writing all of the equations in matrix form. The coefficients of T_s and T_r on the left side of the equations can be written as $\boldsymbol{A_s}$ and $\boldsymbol{A_r}$, which are $n_{Gd} \times n_{Gd}$ coefficient matrices of temperature variables, and the right side of the equations can be written as $\boldsymbol{b_s}$ and $\boldsymbol{b_r}$, which are $n_{Gd} \times 1$ vectors.

TABLE 6. The measurement configurations of IEEE 34-bus electrical network.

Measurement type	branch power	node injection power	node voltage magnitude	branch current magnitude
Number (Three phase)	152	136	9	33

APPENDIX C
MEASUREMENT CONFIGURATIONS

The measurement configuration which is listed in Table 6 of the IEEE 34-bus electrical network does not change in the simulation, and the measurement redundancy is 1.71. The measurement configurations of Barry island heating network under three scenarios are shown in Table 7.

TABLE 7. The measurement configurations of barry island heating network.

Scenario	heat power	pressure	mass flow	temperature	pseudo measurements	redundancy
1A	32	32	64	61	0	2.10
2A	3	32	64	61	0	1.77
3A	3	32	64	61	21	2.01

ACKNOWLEDGMENT

We thank LetPub (www.letpub.com) for its linguistic assistance during the preparation of this manuscript.

REFERENCES

[1] P. Mancarella, "MES (multi-energy systems): An overview of concepts and evaluation models," (in English), *Energy*, vol. 65, pp. 1–17, Feb. 2014.
[2] J. Wu, J. Yan, and H. Jia, "Integrated Energy Systems," *Appl. Energy*, vol. 167, pp. 155–157, 2016.
[3] Q. Chen, J. Hao, and T. Zhao, "An alternative energy flow model for analysis and optimization of heat transfer systems," *Int. J. Heat Mass Transf.*, vol. 108, pp. 712–720, May 2017.
[4] X. Liu, J. Wu, N. Jenkins, and A. Bagdanavicius, "Combined analysis of electricity and heat networks," *Appl. Energy*, vol. 162, pp. 1238–1250, Jan. 2016.
[5] Z. G. Pan, Q. L. Guo, and H. B. Sun, "Interactions of district electricity and heating systems considering time-scale characteristics based on quasi-steady multi-energy flow," *Appl. Energy*, vol. 167, pp. 230–243, Apr. 2016.
[6] Z. Li, W. Wu, J. Wang, B. Zhang, and T. Zheng, "Transmission-constrained unit commitment considering combined electricity and district heating networks," *IEEE Trans. Sustain. Energy*, vol. 7, no. 2, pp. 480–492, Apr. 2016.
[7] S. Chen, Z. Wei, G. Sun, K. W. Cheung, D. Wang, and H. Zang, "Adaptive robust day-ahead dispatch for urban energy systems," *IEEE Trans. Ind. Electron.*, vol. 66, no. 2, pp. 1379–1390, Feb. 2019.
[8] Z. Pan, J. Wu, and M. Abeysekera, "Quasi-dynamic interactions and security control of integrated electricity and heating systems in normal operations," *CSEE J. Power Energy Syst.*, vol. 5, no. 1, pp. 120–129, Mar. 2019.
[9] H. Ren and W. Gao, "A MILP model for integrated plan and evaluation of distributed energy systems," *Appl. Energy*, vol. 87, no. 3, pp. 1001–1014, Mar. 2010.
[10] J. Wang, Z. Wei, B. Yang, Y. Yong, M. Xue, G. Sun, H. Zang, and S. Chen, "Two-stage integrated electricity and heat market clearing with energy stations," *IEEE Access*, vol. 7, pp. 44928–44938, 2019.
[11] R. Li, W. Wei, S. Mei, Q. Hu, and Q. Wu, "Participation of an energy hub in electricity and heat distribution markets: An MPEC approach," *IEEE Trans. Smart Grid*, vol. 10, no. 4, pp. 3641–3653, Jul. 2018.
[12] A. Abur and A. G. Exposito, *Power System State Estimation: Theory and Implementation*. Boca Raton, FL, USA: CRC Press, 2004.
[13] F. C. Schweppe and J. Wildes, "Power system static-state estimation, part I: Exact model," *IEEE Trans. Power App. Syst.*, vol. PAS-89, no. 1, pp. 120–125, Jan. 1970.
[14] C. W. Hansen and A. S. Debs, "Power system state estimation using three-phase models," *IEEE Trans. Power Syst.*, vol. 10, no. 2, pp. 818–824, May 1995.
[15] Y. Liu, A. P. Meliopoulos, L. Sun, and S. Choi, "Protection and control of microgrids using dynamic state estimation," *Protection Control Modern Power Syst.*, vol. 3, no. 1, pp. 1–13, Oct. 2018.
[16] A. Abur and A. G. Exposito, "Bad data identification when using ampere measurements," *IEEE Trans. Power Syst.*, vol. 12, no. 2, pp. 831–836, May 1997.
[17] H. Wei, H. Sasaki, J. Kubokawa, and R. Yokoyama, "An interior point method for power system weighted nonlinear L/sub 1/ norm static state estimation," *IEEE Trans. Power Syst.*, vol. 13, no. 2, pp. 617–623, May 1998.
[18] M. Huang, Z. Wei, G. Sun, T. Ding, H. Zang, and Y. Zhu, "A multi-objective robust state estimator for systems measured by phasor measurement units," *IEEE Access*, vol. 6, pp. 14620–14628, 2018.
[19] M. Göl and A. Abur, "LAV based robust state estimation for systems measured by PMUs," *IEEE Trans. Smart Grid*, vol. 5, no. 4, pp. 1808–1814, Jul. 2014.

[20] T. Fang and R. Lahdelma, "State estimation of district heating network based on customer measurements," *Appl. Thermal Eng.*, vol. 73, no. 1, pp. 1211–1221, Dec. 2014.
[21] J. Dong, Q. Guo, H. Sun, and Z. Pan, "Research on state estimation for combined heat and power networks," in *Proc. IEEE Power Energy Soc. General Meeting (PESGM)*, Jul. 2016, pp. 1–5. doi: 10.1109/PESGM.2016.7742022.
[22] T. Sheng, Q. Guo, H. Sun, Z, Pan, and J. Zhang, "Two-stage state estimation approach for combined heat and electric networks considering the dynamic property of pipelines," *Energy Procedia*, vol. 142, pp. 3014–3019, Dec. 2017.
[23] T. Zhang, Z. Li, Q. H. Wu, and X. Zhou, "Decentralized state estimation of combined heat and power systems using the asynchronous alternating direction method of multipliers," *Appl. Energy*, vol. 248, pp. 600–613, Aug. 2019.
[24] S. Shamshirband, D. Petkovic, R. Enayatifar, A. H. Abdullah, D. Markovic, M. Lee, and R. Ahmad, "Heat load prediction in district heating systems with adaptive neuro-fuzzy method," *Renew. Sustain. Energy Rev.*, vol. 48, pp. 760–767, Aug. 2015.
[25] E. T. Al-Shammari, A. Keivani, S. Shamshirband, A. Mostafaeipour, L. Yee, D. Petkovic, and S. Ch, "Prediction of heat load in district heating systems by support vector machine with firefly searching algorithm," *Energy*, vol. 95, pp. 266–273, Jan. 2016.
[26] B. Bϕhm, S. Ha, and W. Kim, *Simple Models for Operational Optimization*. Lyngby, Denmark: Technical University of Denmark. 2002.
[27] E. Manitsas, R. Singh, B. C. Pal, and G. Strbac, "Distribution system state estimation using an artificial neural network approach for pseudo measurement modeling," *IEEE Trans. Power Syst.*, vol. 27, no. 4, pp. 1888–1896, Nov. 2012.
[28] A. H. Vahabie, M. R. Yousefi, B. N. Araabi, C. Lucas, S. Barghinia, and P. Ansarimehr, "Mutual information based input selection in Neuro-fuzzy modeling for short term load forecasting of Iran national power system," in *Proc. IEEE Int. Conf. Control Automat.*, Jun. 2007, pp. 2710–2715. doi: 10.1109/ICCA.2007.4376854.
[29] A. Abur, "A bad data identification method for linear programming state estimation," *IEEE Trans. Power Syst.*, vol. 5, no. 3, pp. 894–901, Aug. 1990.

HAIXIANG ZANG received the B.S. degree in electrical engineering from Nanjing Normal University, in 2009, and the Ph.D. degree in electrical engineering from Southeast University, in 2014.

He is currently an Associate Professor with the College of Energy and Electrical Engineering, Hohai University, Nanjing, China. His research interests include generation of renewable energy, and operation and control of power system.

MINGHAO GENG received the B.S. degree from Hohai University, Nanjing, China, in 2018, where he is currently pursuing the M.S. degree in electrical engineering. His research interest includes the state estimation of integrated energy systems.

MINGFENG XUE received the B.S. degree from Northwestern Polytechnical University, Xi'an, China, in 1999. He is currently the Deputy Director of Wuxi Power Supply Company of State Grid Jiangsu Electric Power Company Ltd. He is mainly engaged in power system analysis, power demand-side management, load forecasting, and other research work.

XIAOBO MAO received the B.S. degree in electrical engineering from Hohai University, Nanjing, China, in 2015. He is currently a Senior Engineer with the Wuxi Power Supply Company of State Grid Jiangsu Electric Power Company Ltd. He is mainly engaged in integrated energy services and power demand-side management.

MANYUN HUANG received the B.S. degree from the College of Energy and Electrical Engineering, Hohai University, Nanjing, China, in 2014, where she is currently pursuing the Ph.D. degree. From September 2017 to September 2018, she studied at RWTH Aachen University, Germany, as a Joint Ph.D. Student.

Her research interests include the theory and algorithms of power system state estimation and Kalman filter.

SHENG CHEN received the B.S. degree in electrical engineering from the College of Energy and Electrical Engineering, Hohai University, Nanjing, China, in 2014, where he is currently pursuing the Ph.D. degree.

His research interests include integrated energy systems, operations research, and stochastic optimization approaches.

ZHINONG WEI received the B.S. degree from the Hefei University of Technology, Hefei, China, in 1984, the M.S. degree from Southeast University, Nanjing, China, in 1987, and the Ph.D. degree from Hohai University, Nanjing, in 2004.

He is currently a Professor of electrical engineering with the College of Energy and Electrical Engineering, Hohai University. His research interests include power system state estimation, integrated energy systems, smart distribution systems, optimization and planning, load forecasting, and integration of distributed generation into electric power systems.

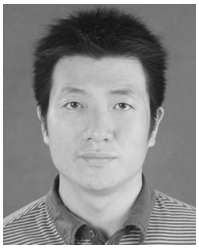

GUOQIANG SUN received the B.S., M.S., and Ph.D. degrees in electrical engineering from Hohai University, Nanjing, China, in 2001, 2005, and 2010, respectively.

He was a Visiting Scholar with North Carolina State University, Raleigh, NC, USA, from 2015 to 2016. He is currently an Associate Professor with the College of Energy and Electrical Engineering, Hohai University. His research interests include power system analysis and economic dispatch, and optimal control of integrated energy systems.